ANESTHESIOLOGY

Propofol Anesthesia Alters Spatial and Topologic Organization of Rat Brain Metabolism

Yali Chen, M.D., Weiqi Bao, M.D., Xia Liang, Ph.D., Jun Zhang, M.D., Ph.D.

ANESTHESIOLOGY 2019; 131:850–65

EDITOR'S PERSPECTIVE

What We Already Know about This Topic

- Graph theory and network analysis have been applied to neuroimaging and neurophysiologic data in the anesthetized state, but there has been little formal analysis of metabolic networks.

What This Article Tells Us That Is New

- The brains of rodents undergoing propofol anesthesia demonstrate reduced metabolic network connectivity and efficiency. These effects might inform the mechanism of the functional disconnections and network inefficiency observed during general anesthesia in humans.

ABSTRACT

Background: Loss of consciousness during anesthesia reduces local and global rate of cerebral glucose metabolism. Despite this, the influence of gradual anesthetic-induced changes on consciousness across the entire brain metabolic network has barely been studied. The purpose of the present study was to identify specific cerebral metabolic patterns characteristic of different consciousness/anesthesia states induced by intravenous anesthetic propofol.

Methods: At various times, 20 Sprague–Dawley adult rats were intravenously administered three different dosages of propofol to induce different anesthetic states: mild sedation (20 mg · kg^{-1} · h^{-1}), deep sedation (40 mg · kg^{-1} · h^{-1}), and deep anesthesia (80 mg · kg^{-1} · h^{-1}). Using [^{18}F]fluorodeoxyglucose positron emission tomography brain imaging, alterations in the spatial pattern of metabolic distribution and metabolic topography were investigated by applying voxel-based spatial covariance analysis and graph-theory analysis.

Results: Evident reductions were found in baseline metabolism along with altered metabolic spatial distribution during propofol-induced anesthesia. Moreover, graph-theory analysis revealed a disruption in global and local efficiency of the metabolic brain network characterized by decreases in metabolic connectivity and energy efficiency during propofol-induced deep anesthesia (mild sedation global efficiency/local efficiency = 0.6985/0.7190, deep sedation global efficiency/local efficiency = 0.7444/0.7875, deep anesthesia global efficiency/local efficiency = 0.4498/0.6481; mild sedation *vs.* deep sedation, global efficiency: $P = 0.356$, local efficiency: $P = 0.079$; mild sedation *vs.* deep anesthesia, global efficiency: $P < 0.0001$, local efficiency: $P < 0.0001$; deep sedation *vs.* deep anesthesia, global efficiency: $P < 0.0001$, local efficiency: $P < 0.0001$). A strong spatial correlation was also found between cerebral metabolism and metabolic connectivity strength, which decreased significantly with deepening anesthesia level (correlation coefficients: mild sedation, $r = 0.55$, deep sedation, $r = 0.47$; deep anesthesia, $r = 0.23$; $P < 0.0001$ between the sedation and deep anesthesia groups).

Conclusions: The data revealed anesthesia-related alterations in spatial and topologic organization of metabolic brain network, as well as a close relationship between metabolic connectivity and cerebral metabolism during propofol anesthesia. These findings may provide novel insights into the metabolic mechanism of anesthetic-induced loss of consciousness.

(ANESTHESIOLOGY 2019; 131:850–65)

General anesthetics are widely used under both clinical and experimental conditions. However, the neurobiologic mechanism of anesthetic-induced unconsciousness is still awaiting further exploration. Early positron emission tomography studies have shown that general anesthetic-induced loss of consciousness is associated with substantial hypometabolism across widespread brain structures,[1–3] suggesting consciousness may be a product of the organization of energetic activity in the brain.[4] In several studies, there were regional metabolic changes in the thalamus, as well as bilaterally in the frontoparietal associative regions, whereas metabolism in the sensory and motor cortices was relatively preserved.[5,6] These regional discrepancies in hypometabolism may imply that cognitive operations are partially suppressed within a hierarchically organized brain network. Indeed, recent theoretical and experimental evidence has suggested that breakdown of brain network interactions during anesthesia, leading to cortical information disintegration and ultimately to loss of consciousness.[6–13] Positron emission tomography and functional magnetic resonance imaging studies in both humans and animals have supported this hypothesis.[14–18]

Supplemental Digital Content is available for this article. Direct URL citations appear in the printed text and are available in both the HTML and PDF versions of this article. Links to the digital files are provided in the HTML text of this article on the Journal's Web site (www.anesthesiology.org). Y.C., W.B., and X.L. contributed equally to this article.

Submitted for publication October 26, 2018. Accepted for publication May 1, 2019. From the Department of Anesthesiology (Y.C.), the Positron Emission Tomography Center (W.B.), and the Department of Anesthesiology (J.Z.), Huashan Hospital, Fudan University, Shanghai, China; and the Laboratory for Space Environment and Physical Science, Harbin Institute of Technology, Harbin, China (X.L.).

 Anesthesiology 2019; 131:850–65. DOI: 10.1097/ALN.0000000000002876

Previous studies have demonstrated that brain functional topology is tightly coupled with cerebral metabolism during awake resting and that cognitive demands modulate this coupling,[19,20] suggesting that changes in brain metabolism are associated with reorganized functional connectivity architecture during changing brain states.[18] However, few studies have directly examined the relationship between brain metabolism and network connectivity at different levels of consciousness.

Interregional connectivity in the resting brain can be detected using fluorodeoxyglucose positron emission tomography, which can measure cerebral metabolism and reflect neuronal activity and viability. Horwitz *et al.*[21] described intersubject metabolic correlations among different brain regions, demonstrating that fluorodeoxyglucose positron emission tomography can reliably identify functionally connected networks. Such methods are now increasingly used to study metabolic connectivity in both the healthy and diseased populations,[22–28] as well as to examine the topologic architecture of the metabolic brain network.

In the present study, we collected fluorodeoxyglucose positron emission tomography data in rats across several levels of propofol-induced anesthesia. We aimed to investigate (1) whether and how the spatial pattern of cerebral metabolism changes when the animal is exposed to an increasing dosage of propofol; (2) whether and how the connectivity architecture of the metabolic brain network reorganizes with changing consciousness/anesthesia level; and (3) whether anesthesia-induced alterations to baseline metabolism are related to changes in metabolic network connectivity and, if so, whether this relationship is modulated by changes in consciousness/anesthesia level.

Materials and Methods

Animal Preparation

A total of 23 adult male Sprague–Dawley rats aged 8 to 10 weeks and weighing 300 to 350 g were acquired from Shanghai Sippr-BK Laboratory Animal Co. Ltd. (China) for use in the present study. The animals were housed in a temperature- (21 ± 1°C) and humidity-controlled (45 to 60%) facility with a 12/12-h reverse light–dark cycle. They had *ad libitum* access to food and water. The present study protocol was approved by the Fudan University Animal Care and Use Committee of Medical College (Shanghai, China) and was conducted in compliance with the Guide for the Care and Use of Laboratory Animals.

Experimental Protocol

Fluorodeoxyglucose positron emission tomography data were acquired from each rat during the daytime at three different levels of anesthesia induced by propofol dosages of 20, 40, and 80 mg · kg^{-1} · h^{-1}. Before positron emission tomography scanning, the rats were fasted for 12 h. They then underwent tail vein cannulation while immobilized in the prone position with a rat fixator. The experimental procedure is summarized in figure 1. A randomized crossover method was used to avoid bias in anesthetic dosage administration. No blinding methods were used during fluorodeoxyglucose positron emission tomography data acquisition. Briefly, to reach steady state, we intravenously infused propofol at a rate of either 20, 40, or 80 mg · kg^{-1} · h^{-1} for 15 min using a syringe pump (B. Braun, Germany). During the infusion, 1 l/min oxygen was delivered *via* a catheter around the rat's nose, and an infrared heating lamp (Xupurui Lighting Source Manufacture Co., Ltd., China) was used to avoid hypothermia. The rat's behavioral response was tested using the righting reflex, and then each animal was injected with less than 1 ml of [^{18}F]fluorodeoxyglucose (1 mCi) through the tail vein. After a 40-min uptake period[29] involving continued propofol infusion, the rats were transferred and fixed to the micro–positron emission tomography/computed tomography scanner frame, inspiring a mixture of 1% isoflurane in 30% oxygen gas. After scanning, the animals were returned to their cages. The positron emission tomography scans were repeated in each rat at another two sessions 3 days apart according to a predefined order of propofol dosage (40/80/20 and 80/20/40 mg · kg^{-1} · h^{-1}).

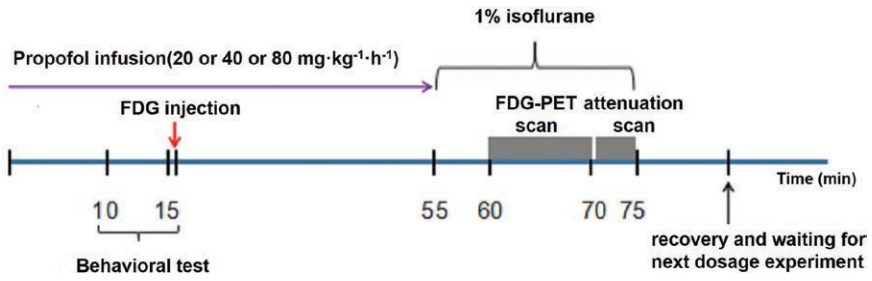

Fig. 1. Time course of small animal positron emission tomography (PET) scanning during three different levels of propofol-induced anesthesia at dosages of 20, 40, and 80 mg · kg^{-1} · h^{-1}. FDG, fluorodeoxyglucose.

Measurement of Physiologic Parameters

Vital signs and blood biochemical parameters were examined outside the scanner in a subgroup of rats (n = 3) at the three different propofol dosages. Local anesthesia with 2% lidocaine was administered subcutaneously to allow femoral artery cannulation. After tail-vein cannulation, the rats were intravenously infused with propofol (administered sequentially: 20, 40, and 80 mg · kg^{-1} · h^{-1}). Invasive arterial blood pressure and heart rate were measured using a connected monitor (Datex–Ohmeda, USA). An arterial blood sample (0.5 ml) was drawn 15 min after the start of propofol infusion at each dosage to measure the arterial oxygen and carbon dioxide tension (Pa_{O_2} and Pa_{CO_2}), pH, and glucose levels using a blood gas analyzer (ABL 900, Radiometer, Denmark).

Behavioral Test and Electroencephalogram Monitoring

To define the anesthesia state at different propofol infusion rates, we performed both behavioral testing, as described in previous studies,[30,31] and scalp electroencephalogram monitoring in a subgroup of three rats. First, we assessed behavioral response using the righting reflex: the animal was placed on its side, and its attempts to right itself were observed.[32] An animal that made no righting attempt was considered unconscious. The test procedure was repeated three times at each propofol dosage 15 min after propofol infusion. In addition, we acquired electroencephalogram scalp recordings using needle electroencephalogram electrodes and electroencephalogram recorder software (EBNeuro, Italy). The electroencephalogram electrodes were placed as follows: two on the frontal region, two on the temporal region, one reference electrode at the base of the nose, one ground electrode on the left forelimb, and one electrocardiogram electrode on the left chest. The recording parameters during collection were as follows: sampling rate of 5,000 Hz per channel, resistance of less than 20 MΩ, and band-pass filter between 2 and 150 Hz.

Positron Emission Tomography Data Acquisition

Positron emission tomography data were acquired for about 10 min using a Siemens Inveon MM microposition emission tomography/CT scanner (Siemens Medical Solutions, USA). Using emission acquisition, the energy window was 350 to 650 keV, with a time window of 3.432 ns. This was followed by an attenuation correction CT scan in the same machine (exposure time of 250 ms, voltage of 80 kV, current of 500 mA, field of view of 3,072 × 2,048, binning of 4, low resolution, three beds, and overlap ratio of 36.44%). The images were reconstructed using the ordered subsets expectation maximization algorithm, with attenuation, scatter, and random correction. The final voxel size of the image was 0.776 × 0.776 × 0.796 mm^3.

Positron Emission Tomography Data Preprocessing

Spatial processing was performed using PMOD 3.4 software (PMOD Technology, Switzerland) and Analysis of Functional NeuroImages (http://afni.nimh.nih.gov/afni. Accessed April 30, 2018). The reconstructed positron emission tomography images were first coregistered to the [^{18}F]fluorodeoxyglucose rat brain template (Schiffer template) in the fusion module. The Schiffer template was then affine-transformed to the minimal deformation template generated by Valdés-Hernández *et al.*,[33] the transformation matrix of which was used to bring the coregistered fluorodeoxyglucose positron emission tomography images into the minimal deformation template space. After spatial smoothing (full width of half-maximum of 1.2 mm) to increase the signal-to-noise ratio, the fluorodeoxyglucose positron emission tomography images were scaled using the mean fluorodeoxyglucose value within the cerebellum to correct for variability in injection activity. The resulting fluorodeoxyglucose positron emission tomography data (expressed as standardized uptake value ratios) were used for further analysis.

Spatial Variability and Similarity in Brain Metabolism

To explore changes in interregional variability induced by the different propofol dosages, we assessed the spatial variability of brain metabolism in each rat by calculating the SD of the fluorodeoxyglucose value across gray-matter voxels, which is similar to the SD of blood oxygen level-dependent signaling, as shown by functional magnetic resonance imaging studies describing the variance of brain activity within a particular region across time.[34,35] To directly compare the spatial pattern of brain metabolism[36,37] among the different propofol-induced consciousness states, we computed between-state similarity at both group and individual levels. For spatial similarity at the group level, we averaged the standardized uptake value ratio maps across rats within each state; we then computed between-state similarity by calculating the Pearson correlation coefficient of the group-averaged standardized uptake value ratio values between every state pair. To ascertain spatial similarity at the individual level, we computed the voxel-based correlation in standardized uptake value ratio value between different states in each rat. In addition, we calculated spatial variability and similarity at the regional level to account for possible overestimation of correlations.

Metabolic Connectivity Strength Analysis

To identify the metabolic hubs of the whole-brain network, we computed voxel-wise metabolic connectivity strength, which determines the extent to which the standardized uptake value ratio at any particular voxel is correlated with the standardized uptake value ratio of all other cortical voxels. The metabolic connectivity between any two gray-matter voxels was computed by calculating the Pearson correlation coefficients of the standardized uptake value ratio values

across all rats at the group level during each anesthesia state. In particular, the standardized uptake value ratio values for each voxel from each rat were compiled into separate vectors, and the intervoxel Pearson correlation coefficients were calculated for each pair of voxels. We applied a range of correlation thresholds ($0 < r < 0.8$) to eliminate weak correlations that may have arisen from spurious sources of noise. Given that our findings were consistent across different correlation thresholds (Supplemental Digital Content, fig. S1, http://links.lww.com/ALN/B996), we presented the results at a cutoff threshold of 0.4 in the main text. The metabolic connectivity strength at a given voxel was then defined as the sum of the weights of its metabolic connectivity to all other gray-matter voxels. Voxels with high metabolic connectivity strength (more than the mean of 1 SD) were identified as metabolic hubs because they had high metabolic connectivity to the rest of the brain. To examine whether changes in metabolic connectivity strength are related to alterations in metabolic activity, we calculated the spatial correlation between metabolic connectivity strength and the standardized uptake value ratio across voxels at each of the three anesthesia states.

Energy Efficiency Analysis

To evaluate the efficiency of glucose use during functional communication, we analyzed energy efficiency during the different anesthesia states by calculating the ratio between metabolic connectivity strength and standardized uptake value ratio at both the voxel-wise and region-wise levels.[20,38]

Metabolic Network Analysis

To ensure computational efficiency during network analysis and permutation tests, we calculated the network efficiency metrics at the regional level by parcellating the rat brain into 110 regions based on the combined atlas provided by Valdés-Hernández *et al.*,[33] Schwarz *et al.*,[39] and Calabrese *et al.*[40] In each of the three propofol groups, a correlation matrix was constructed by calculating the Pearson correlation coefficient of the average standardized uptake value ratio between any pair of brain regions across each rat. All the resulting network properties were computed on weighted matrices using weight-conserving algorithms.[41] Before metabolic network analysis, the connectivity matrices were thresholded using the false discovery rate to avoid nonsignificant links, with a threshold false discovery rate of less than 0.05 for multiple-comparison correction. To explore the influence of thresholding on small-world attributes, the small-world analysis was repeated at different correlation thresholds ($0.1 \le r \le 0.9$, with an incremental interval of 0.1) and network densities ($0.1 \le \kappa \le 0.9$, with an incremental interval of 0.1).

The global and local efficiencies were calculated at the group level using the Gretna Toolbox.[42] These values were then used to measure how efficiently parallel information was exchanged over wide-scope and local brain regions, as described by Latora and Marchiori.[43] Small-world networks have high global and local efficiency, representing efficient global and local communication.

Global efficiency is commonly defined as the inverse, average shortest path length as follows:

$$E_{global} = \frac{1}{N(N-1)} \sum_{i \neq j \in G} \frac{1}{d_{ij}}$$

where N is the number of nodes in the graph G, and d_{ij} is the shortest path length between node i and node j.

Local efficiency plays a similar role to the clustering coefficient of the network,[44] as estimated by the following formula:

$$E_{local} = \frac{1}{N} \sum_{i \in G} E(G_i)$$

where G_i is the subgraph of the neighbors of node i without including node i. Local efficiency indicates how efficient communication is between the first neighbors of i when i is removed.

To evaluate the small-worldness of each metabolic network, the normalized small-world parameters N (global efficiency) and N (local efficiency) were computed from the average parameters of 500 randomly rewired null-model networks. These random networks were generated using the random rewiring procedure described by the Markov-chain algorithm,[45,46] which preserves the same number of nodes and edges as real brain metabolism networks, as well as the same degree distribution. Typically, classical small-world topology should have a normalized global efficiency of approximately 1 and a normalized local efficiency of more than 1.

Statistical Analysis

The sample size was based on previous studies into rat brain metabolism and metabolic networks[47] rather than on a calculation of statistical power. Two-sided *P* values of less than 0.05 were considered statistically significant.

To evaluate the effect of propofol dosage on brain metabolism, one-way repeated-measures ANOVA, with propofol dosage as the within-subject factor, was applied to the standardized uptake value ratio of glucose; this was followed by *post hoc*, independent, two-sample *t* tests between every pair of groups (Analysis of Functional NeuroImages, http://afni.nimh.nih.gov/afni). The group difference maps were first thresholded with a voxel-wise significance of $P < 0.05$. A multiple comparison correction was then carried out using a cluster size threshold of 675 voxels derived from Monte Carlo simulations to reach a cluster level significance of $P < 0.05$ (AlphaSim correction in Analysis of Functional NeuroImages). To test whether the effect of propofol varied between cortical and subcortical regions, a two-way, repeated-measures ANOVA (factor "propofol dosage": 20, 40, and 80 mg · kg^{-1} · h^{-1}; factor "region":

cortex and subcortex) was performed on the standardized uptake value ratio averages within the cortical and subcortical regions, with dosage as the between-subject factor and region as the within-subject factor (IBM SPSS Statistics, version 17). η^2 was used to measure the effect size.[48]

A preplanned, independent, two-sample *t* test was applied to the spatial variability between the different propofol dosages, and Bonferroni-corrected *P* values of less than 0.05 were considered statistically significant in multiple comparisons. A one-way, repeated-measures ANOVA, with propofol dosage as the within-subject factor, was applied to spatial similarity at the individual level, followed by independent, *post hoc*, two-sample *t* tests between every pair of groups (IBM SPSS Statistics, version 17).

To analyze spatial similarity at the group level, the correlation coefficient between metabolic connectivity strength and standardized uptake value ratio, and the metabolic connectivity metrics (energy efficiency, global efficiency, and local efficiency), a nonparametric permutation test was used, whereby dosage-related differences were evaluated using Matlab R2016a software. A total of 10,000 random permutations were generated independently; for each permutation, the standardized uptake value ratios of the images were randomly permuted across the three groups, and the test statistic of interest was recalculated, yielding a distribution of 10,000 values from the permuted data. The *P* value was determined by comparing the observed value with the permutation-generated distribution.[38] This procedure was applied each time a permutation test was performed in the analysis. For multiple comparisons, Bonferroni-corrected *P* values of less than 0.05 were considered statistically significant for the metrics including correlation coefficient between metabolic connectivity strength and standardized uptake value ratio, global efficiency and local efficiency. We used the false discovery rate method at a threshold false discovery rate of less than 0.05 for multiple-comparison correction of metabolic connectivity and energy efficiency in each brain region.

Results

In total, we acquired 60 positron emission tomography images from 20 rats. Among them, three scans in the 40 mg · kg^{-1} · h^{-1} group were excluded because the images were blurred. Thus, spatial and topologic analyses of rat brain metabolism were applied to 57 positron emission tomography images under three levels of anesthesia: 20 scans in the 20 mg · kg^{-1} · h^{-1} group, 17 in the 40 mg · kg^{-1} · h^{-1} group, and 20 in the 80 mg · kg^{-1} · h^{-1} group.

Physiologic Variables, Behavior, and Electroencephalogram Activity

The physiologic measurements acquired 15 min after propofol infusion are shown in table S1 of the Supplemental Digital Content (http://links.lww.com/ALN/C4). Higher dosages of propofol were associated with decreased mean arterial blood pressure and heart rate, whereas pH, $P_{A}O_2$, $P_{A}CO_2$, and blood glucose levels remained unchanged among the three propofol dosages. Based on the animals' behavioral performance and electroencephalogram characteristics (Supplemental Digital Content, fig. S2, http://links.lww.com/ALN/B997, shows the raw electroencephalogram traces), we defined the anesthesia states induced by the different propofol dosages as follows (Supplemental Digital Content, table S2, http://links.lww.com/ALN/C4): mild sedation (20 mg · kg^{-1} · h^{-1} propofol), as evidenced by low-amplitude and high-frequency electroencephalogram activity, as well as the existence but slow response to righting reflex; deep sedation (40 mg · kg^{-1} · h^{-1}), as evidenced by lower frequency and higher amplitude electroencephalogram activity, as well as loss of righting reflex in some animals; and deep anesthesia (80 mg · kg^{-1} · h^{-1}), as evidenced by high amplitude, low-frequency waves mixed with spiked or sharp waves, and occasional burst suppression, as well as loss of righting reflex in all animals.

Global Reduction in Brain Metabolism during Propofol Anesthesia

We first compared the standardized uptake value ratios among the three anesthesia states to elucidate any dosage-related changes in brain metabolic activity. We found that brain metabolism decreased gradually with increasing dosage of propofol (fig. 2A). Specifically, in deep sedation, global brain metabolism was lower than in mild sedation across widely distributed cortical and subcortical areas (corrected $P < 0.05$, using Monte Carlo simulations; fig. 2B). In contrast, when comparing deep anesthesia with deep sedation, decreases in metabolism were more evident in the cortical than in the subcortical regions. This observation was further confirmed by two-way ANOVA (between-subject factor "propofol dosage": 20, 40, 80 mg · kg^{-1} · h^{-1} and within-subject factor "region": cortex and subcortex), which showed a significant main effect of dosage (F_{dosage} [2,54] = 85.64, $\eta^2 = 0.75$; $P < 0.0001$), as well as a significant interaction effect between dosage and region ($F_{dosage*region}$ [2,54] = 63.46, $\eta^2 = 0.53$; $P < 0.0001$; fig. 2C), indicating that brain metabolism in the cortical and subcortical regions is affected differently by increasing propofol dosages. Furthermore, the propofol-induced reduction in brain metabolism was closely related to initial metabolic level (standardized uptake value ratio $[SUVr]_{mild\ sedation–deep\ sedation}$ correlates with $SUVr_{mild\ sedation}$: $r = 0.79$, $P < 0.0001$, and 95% CI, 0.782 to 0.791; $SUVr_{deep\ sedation-deep\ anesthesia}$ correlates with $SUVr_{deep\ sedation}$: $r = 0.65$, $P < 0.0001$, and 95% CI, 0.645 to 0.658; $SUVr_{mild\ sedation-deep\ anesthesia}$ correlates with $SUVr_{mild\ sedation}$: $r = 0.84$, $P < 0.0001$, and 95% CI, 0.839 to 0.846; fig. 2D).

Propofol Altered the Spatial Variability and Spatial Similarity of Brain Metabolism with Increasing Dosage

To assess whether propofol-induced reductions in glucose consumption were accompanied by alterations in its spatial

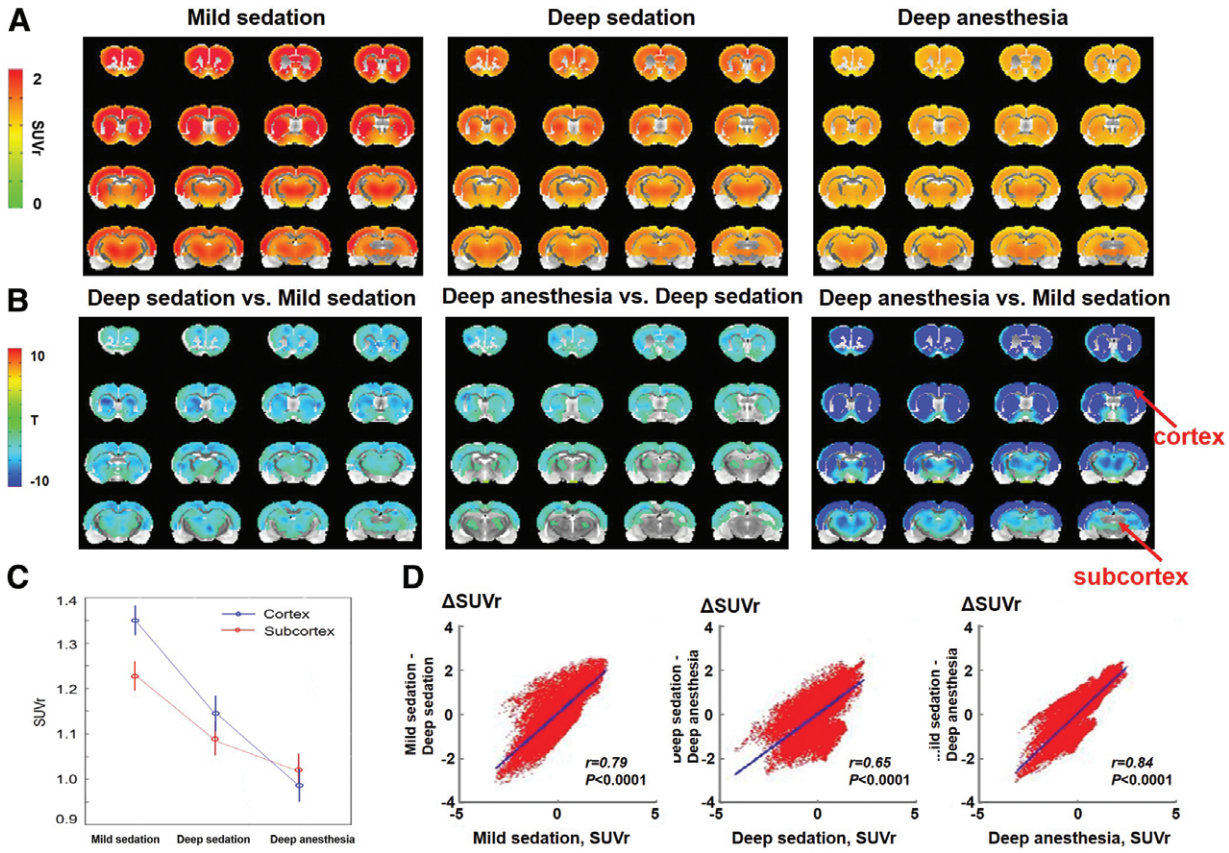

Fig. 2. Propofol-induced reduction in glucose metabolic rate. (*A*) Spatial distribution of brain metabolism (standardized uptake value ratio [SUVr]) during different propofol anesthesia states. A voxel-wise mean metabolism map was calculated by averaging the metabolism map across all rats in each state. (*B*) Statistically significant decreases in SUVr across widespread brain regions between different consciousness states (corrected $P < 0.05$, using Monte Carlo simulations). Decreases in metabolism are more evident in the cortex than in the subcortical regions, especially when comparing deep sedation with deep anesthesia. (*C*) Two-way ANOVA analysis revealed significant main effects of propofol dosage, as well as an interaction effect between dosage and region, confirming that propofol has distinct effects in the cortical and subcortical regions. (*D*) Scatterplot of the relationship across voxels between changes in brain metabolism and initial cerebral metabolic level.

distribution, we computed spatial variation and spatial similarity. The spatial variability of brain metabolism indicates anatomical variation in metabolism across the whole brain. Comparisons among different anesthesia states revealed significantly reduced spatial variability in brain metabolism with increasing propofol dosage after Bonferroni's correction for multiple comparisons (spatial variability [mean ± SD]: mild sedation, 0.192 ± 0.019; deep sedation, 0.150 ± 0.023; deep anesthesia, 0.120 ± 0.014; independent two-sample *t* test, mild sedation *vs.* deep sedation, $t = 6.32$, $P < 0.0001$, Cohen's d = 2.07; deep sedation *vs.* deep anesthesia, $t = 4.87$, $P < 0.0001$, Cohen's d = 1.65; mild sedation *vs.* deep anesthesia, $t = 13.96$, $P < 0.0001$, Cohen's d = 4.37; fig. 3A), suggesting that glucose metabolism tends to converge to a similar level in different brain regions during propofol-induced anesthesia. Spatial similarity in brain metabolism was examined to directly compare metabolism distribution between different anesthesia states. The results at group level showed that the mild sedation/deep sedation between-state spatial similarity ($r = 0.927$, $P < 0.0001$; 95% CI, 0.926 to 0.929) was statistically significantly higher (nonparametric permutation test: $P < 0.0001$) than the mild sedation/deep anesthesia spatial similarity ($r = 0.63$, $P < 0.0001$; 95% CI, 0.627 to 0.641) and the deep sedation/deep anesthesia spatial similarity ($r = 0.80$, $P < 0.0001$; 95% CI, 0.799 to 0.807; fig. 3B). At the individual level, spatial similarity was performed on data from 17 rats; three images in the deep sedation group were excluded because they were blurred. The statistical analysis was consistent with that at group level (spatial similarity [mean ± SD]: mild sedation correlates with deep sedation, $r = 0.72 \pm 0.12$; deep sedation correlates with deep anesthesia, $r = 0.53 \pm 0.23$; mild sedation correlates with deep anesthesia: $r = 0.36 \pm 0.25$, $F[2,48] = 19.9$, $P < 0.0001$; fig. 3C). There was significantly weakened spatial similarity between the mild sedation and deep anesthesia states, indicating that the spatial pattern of brain metabolism in

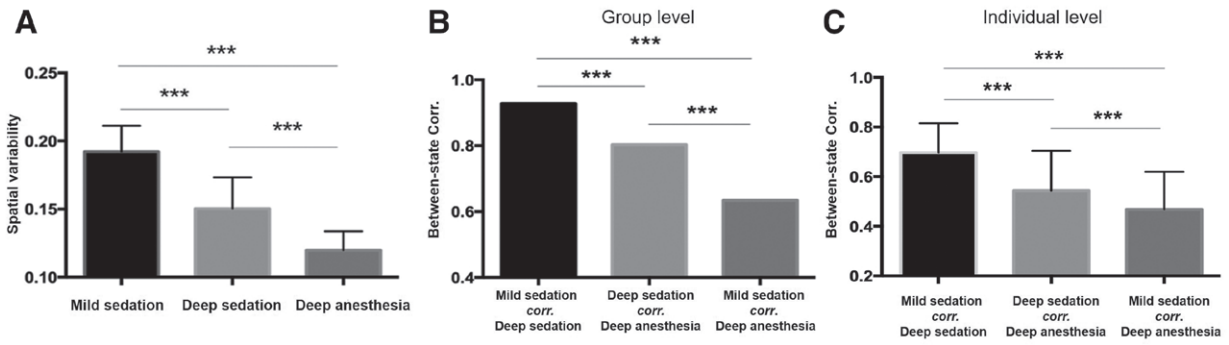

Fig. 3. Spatial variability and spatial similarity in brain metabolism. (*A*) Spatial variability of brain metabolism decreases as the level of anesthesia deepens. (*B*) Between-state similarity in brain metabolism at the group level. (*C*) Between-state similarity in brain metabolism at the individual level. ***$P < 0.05/3$ (with Bonferroni's correction [*corr.*]).

deep anesthesia differed markedly from that in sedation states. Note that the voxel-wise level observations of spatial variation and spatial similarity in brain metabolism remained consistent in regional-wise analyses (Supplemental Digital Content, fig. S3, http://links.lww.com/ALN/B998), confirming that these findings were robust.

Propofol Decreased the Spatial Correlation between Brain Metabolism and Hub Connectivity with Increasing Dosages

The above results showed changes in brain glucose metabolism during propofol-induced anesthesia. Because previous evidence has indicated that brain metabolism is closely connected to functional connectivity hubs in both resting and task states, we next explored whether the relationship between brain metabolism and connectivity strength would be preserved during anesthesia and modulated by propofol load. Metabolic connectivity strength was computed at the voxel level. That is, the average metabolic connectivity was calculated between a given voxel and all other voxels in the rat brain. In mild and deep sedation states, metabolic hubs with high metabolic connectivity strengths were primarily distributed in the anterior cingulate cortex, medial prefrontal cortex, retrosplenial cortex, parietal association cortex, primary/secondary motor and somatosensory cortices, temporal association cortices, and striatum (fig. 4A), overlapping with the key components of the default mode network. In contrast, during deep anesthesia, metabolic connectivity strength decreased in the midline cortical regions of the medial prefrontal and retrosplenial cortices, and several subcortical regions in the diencephalon and striatum arose as metabolic hubs with elevated standardized uptake value ratio values (fig. 4, A and B; Supplemental Digital Content, fig. S1, http://links.lww.com/ALN/B996; and fig. S4, http://links.lww.com/ALN/B999). The spatial pattern of these metabolic hubs resembled the distribution of brain regions with high glucose metabolism. Indeed, correlation analysis across all voxels showed a striking spatial overlap between metabolic connectivity strength and standardized uptake value ratio during all three anesthesia states (mild sedation: $r = 0.55$, $P < 0.0001$, and 95% CI, 0.543 to 0.559; deep sedation: $r = 0.48$, $P < 0.0001$, and 95% CI, 0.471 to 0.489; deep anesthesia: $r = 0.23$, $P < 0.0001$, and 95% CI, 0.222 to 0.244). The between-state permutation tests revealed a significant reduction in the correlation between metabolic connectivity strength and standardized uptake value ratio from mild sedation to deep anesthesia (nonparametric permutation test: $P < 0.0001$) and from deep sedation to deep anesthesia (nonparametric permutation test: $P = 0.014$; fig. 4C; Supplemental Digital Content, fig. S5, http://links.lww.com/ALN/B1000), indicating that the coupling between metabolic connectivity strength and standardized uptake value ratio was modulated by propofol dosage.

Decrease in Energy Efficiency during Propofol Anesthesia

To evaluate the energy demands of neural communication and investigate energy efficiency at different anesthesia states, we further computed the ratio between metabolic connectivity strength and standardized uptake value ratio in each voxel. Energy efficiency was high in most cortical regions, including the anterior cingulate cortex, medial prefrontal cortex, retrosplenial cortex, parietal association cortex, and primary/secondary motor and somatosensory cortices, as well as in a few subcortical regions, including the striatum, diencephalon, and pallidum (fig. 5, A and B; Supplemental Digital Content, fig. S6, http://links.lww.com/ALN/C2). Because it is difficult to perform a comparison at the voxel-wise level, we further computed energy efficiency at the region-wise level and compared it between states. As shown in Figure 5C, under deep anesthesia, markedly lower energy efficiency was found than under either mild or deep sedation, mainly in the left medial prefrontal

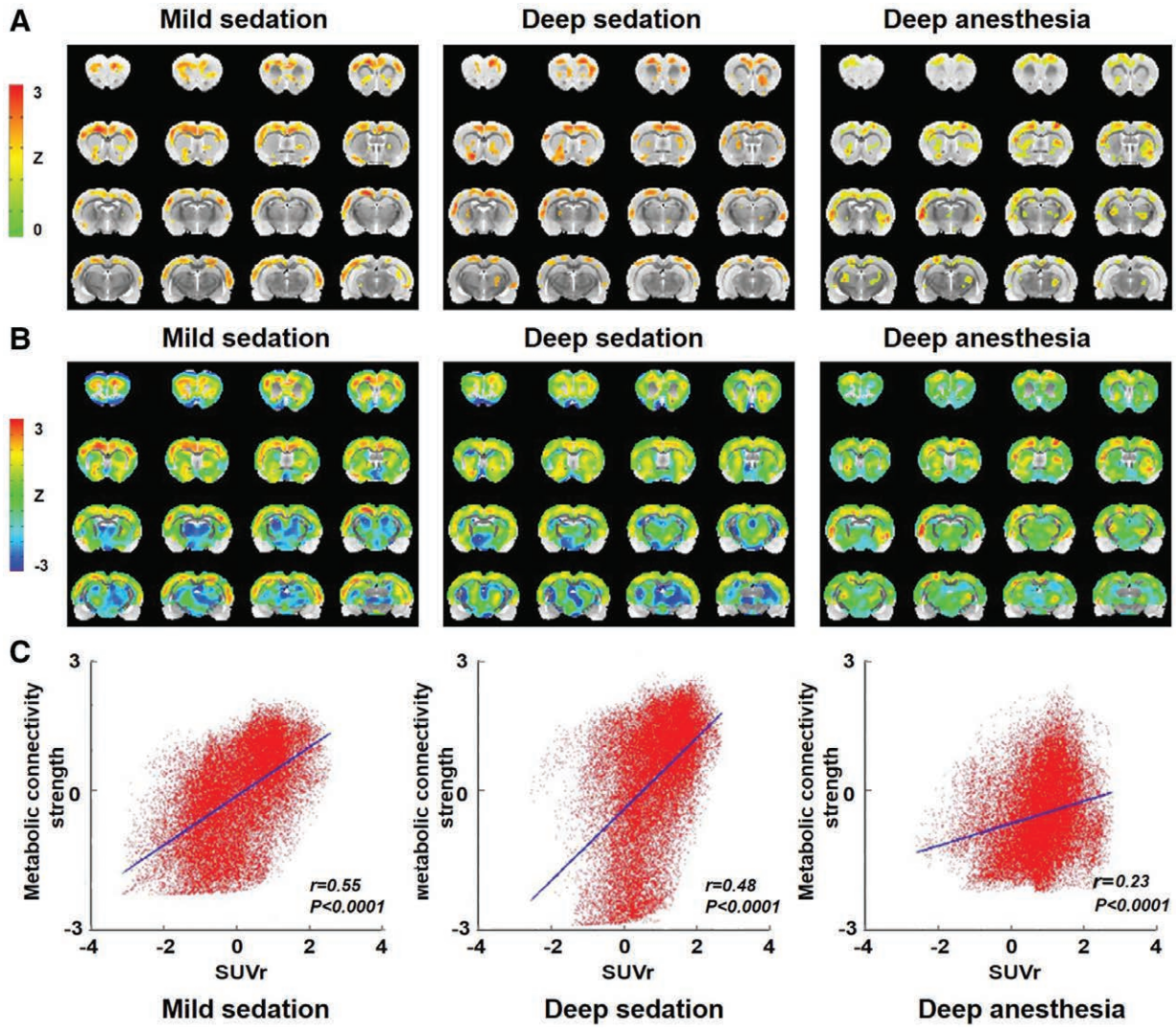

Fig. 4. Spatial distribution of metabolic connectivity strength and relationship between metabolic connectivity strength and metabolism during three propofol anesthesia states. (*A*) Metabolic hubs are shown. (*B*) Spatial distribution of metabolic connectivity strength. (*C*) Scatterplot of the relationship between metabolic connectivity strength and metabolism (represented as standardized uptake value ratio [SUVr]) across voxels.

cortex, retrosplenial cortex, primary somatosensory cortex, primary visual cortex, pallidum, and left diencephalon (uncorrected $P < 0.001$); a marginal reduction was found in the right medial prefrontal cortex, primary somatosensory cortex, right diencephalon, left hypothalamus, and amygdala (uncorrected $P < 0.005$). No changes in energy efficiency were found between the mild sedation and deep sedation states except for amygdala and pallidum.

Propofol Modulated the Topologic Organization of the Metabolic Brain Network

To assess whether propofol-induced anesthesia changes the topologic organization of the metabolic brain network, we estimated metabolic network connectivity and efficiency at the region-wise level during the different consciousness levels. The results showed that metabolic connectivity among several regions was significantly stronger during deep sedation than during mild sedation (1,172 of 5,578 [21%] of all connectivity pairs; false discovery rate corrected at $P < 0.05$; fig. 6, A through C) but significantly weaker during deep anesthesia than during the other two consciousness states across a wide range of brain regions (3,960 of 5,578 [71%] of all connectivity pairs; fig. 6, A through C). Moreover, there were more dosage-dependent differences in the number of connections among the various cortical regions than among the cortico–subcortical and subcortical regions (fig. 6C; Supplemental Digital Content, table S3, http://links.lww.com/ALN/C4).

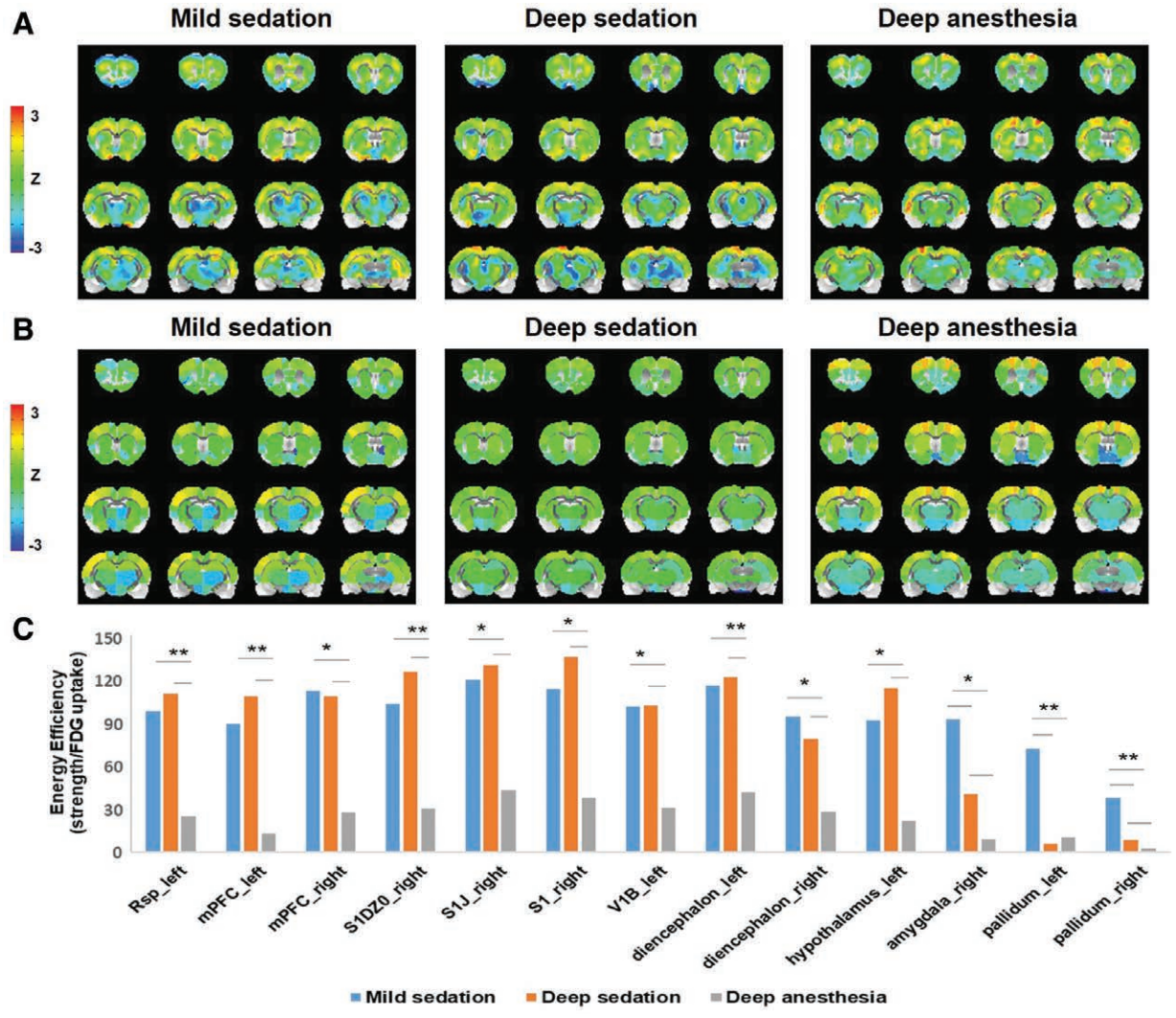

Fig. 5. Reduced energy efficiency at deep anesthesia state. We defined energy efficiency as the ratio between metabolic connectivity strength and standardized fluorodeoxyglucose (FDG) uptake (standardized uptake value ratio) in each region. (*A*) Spatial distribution of voxel-wise energy efficiency. (*B*) Spatial distribution of region-wise energy efficiency. (*C*) The bar chart shows regions with significant differences in energy efficiency between deep anesthesia and mild/deep sedation. *Uncorrected $P < 0.005$; **Uncorrected $P < 0.001$. SUVr, Rsp_left, retrosplenial cortex; mPFC_left, medial prefrontal cortex; S1DZ0_right/S1J_right/S1_right, primary somatosensory cortex; V1B_left, primary visual cortex.

The rat metabolic brain network showed a classical small-world topology under all three anesthesia states (normalized global efficiency of approximately 1, normalized local efficiency of more than 1). Nevertheless, there were significant between-state differences in the small-world efficiency parameters: both global efficiency and local efficiency were significantly lower under deep anesthesia than under either mild or deep sedation. No significant differences were found between mild sedation and deep sedation in this regard (mild sedation global efficiency/local efficiency of 0.6985/0.7190, deep sedation global efficiency/local efficiency of 0.7444/0.7875, deep anesthesia global efficiency/local efficiency of 0.4498/0.6481; nonparametric permutation test: mild sedation *vs.* deep sedation, global efficiency: $P = 0.356$, local efficiency: $P = 0.079$; mild sedation *vs.* deep anesthesia, global efficiency: $P < 0.0001$, local efficiency: $P < 0.0001$; deep sedation *vs.* deep anesthesia, global efficiency: $P < 0.0001$, local efficiency: $P < 0.0001$; fig. 6D and Supplemental Digital Content, fig. S7, http://links.lww.com/ALN/C3).

Discussion

Using [^{18}F]fluorodeoxyglucose micro–positron emission tomography, the present study demonstrated significant

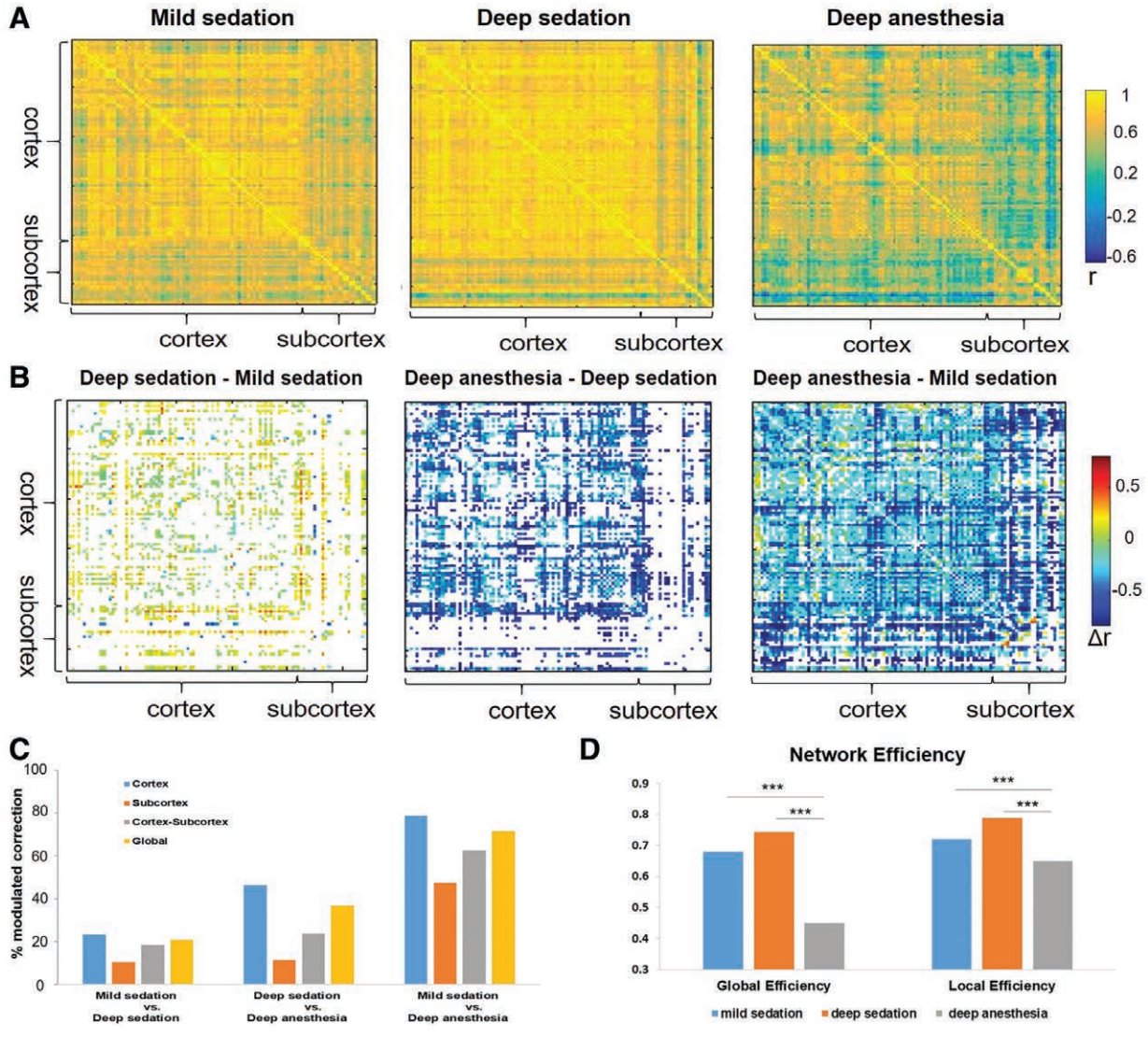

Fig. 6. Metabolic connectivity between regions and network efficiency during three anesthesia states. (*A*) Metabolic connectivity matrix constructed for three anesthesia states. (*B*) Contrast maps showing regions that changed significantly in metabolic connectivity between the different anesthesia states (nonparametric permutation test; $P < 0.05$ with false discovery rate correction). (*C*) The percentage of significantly changed connections among the different regions (cortex–cortex, cortex–subcortex, subcortex–subcortex, and global) between states. The percentage values are based on the sum of the significantly modulated connections observed, scaled by total number of possible connections. (*D*) Global and local efficiency were significantly lower at deep anesthesia than in the mild and deep sedation states. ***$P < 0.05/3$ with Bonferroni's correction, using the nonparametric permutation test.

reductions in baseline metabolism alongside altered metabolic spatial distribution during propofol-induced anesthesia. Moreover, based on graph-theory analysis, we revealed disruptions to both global and local efficiency of the metabolic brain network, characterized by decreases in metabolic connectivity and energy efficiency during propofol-induced deep anesthesia. We also found a strong spatial correlation between cerebral metabolism and metabolic network connectivity; this decreased significantly as the level of anesthesia deepened. These findings provide compelling evidence that the changes in brain metabolism are associated with functional brain network breakdown during loss of consciousness induced by propofol anesthesia. Our findings may contribute to a deeper understanding of the neural correlates of consciousness, and they have clinical implications, particularly in the differential diagnosis and outcome prediction in patients with disorders of consciousness.[49] For instance, partially preserved specific network metabolism may indicate the presence of covert consciousness.[50]

In accordance with previous studies,[1–3,51–53] we found prominent metabolic decreases in widely-distributed

brain regions during high-dosage propofol administration. Interestingly, glucose metabolism decreased more markedly in the cortical than in the subcortical areas with deepening anesthesia level. This difference in metabolic change between the cortical and subcortical regions was also reflected in the metabolic distribution during different anesthesia states. Although metabolism in the cortex was higher than in the subcortex under mild sedation, a contrasting pattern of higher metabolism in the subcortical regions was observed at deeper levels of anesthesia, indicating a spatial shift in glucose metabolism from the cortical to the subcortical regions during deep anesthesia.[54]

Moreover, our results showed that changes in energy consumption during higher propofol dosage (40 and 80 mg · kg^{-1} · h^{-1}) correlated significantly with initial metabolic levels across all brain regions. That is, higher initial metabolic levels in a given brain region were associated with greater decreases in metabolic cost with increasing propofol dosage, suggesting that brain regions of high metabolic demand are more vulnerable to deepened anesthesia with propofol. These hierarchical changes in glucose metabolism across different brain regions were further evidenced because the spatial variation in brain metabolism was gradually attenuated from mild sedation through deep sedation to deep anesthesia. These observations corroborate previous isoflurane studies showing that cerebral metabolism became more uniform across the whole brain during anesthesia, in contrast with the awake state.[55,56]

Propofol potentiates γ-aminobutyric acid type A ($GABA_A$) receptor–mediated postsynaptic inhibition,[57,58] so its effect may depend on the regional distribution of $GABA_A$ receptors[59] and may therefore give rise to differing metabolism changes in various brain regions. Future studies will be needed to directly evaluate this mechanism by monitoring both γ-aminobutyric acid and metabolic activity during propofol anesthesia.

Similarly to functional connectivity, metabolic connectivity,[38] as measured in terms of interregional metabolic correlations in glucose uptake, which can be estimated using fluorodeoxyglucose positron emission tomography, reflects interregional covariance patterns in neuronal activities.[60,61] Previous studies have shown that the metabolic connectivity is a sensitive marker of individual variability in cognitive functioning under both normal conditions and disease.[60,62–64] In the current study, we found wildly decreased metabolic connectivity during deep anesthesia, which is consistent with several previous functional magnetic resonance imaging studies in general anesthesia,[65–67] which suggested that interregional metabolism synchronization is impaired, reducing communication between brain regions during anesthesia.[7] Interestingly, metabolic connectivity increased from mild sedation to deep sedation, suggesting complicated changes in brain functional connectivity between these two states, specifically partial preservation or even increases in some specific networks.[9,18,68] Considering that brain activity is coupled with metabolic flux, the increasing uniform state of metabolic activity across the whole brain with deepening anesthesia may suggest that brain activity is more synchronized in such states, consistent with previous studies showing that a disrupted balance between network segregation and integration is associated with impairment to higher brain functions like cognition and consciousness.[10,69] Furthermore, in line with our observation of divergent changes to regional metabolism between the cortical and subcortical areas, the number of reduced metabolic connections among cortical regions appeared to be larger than that among cortico–subcortical and subcortical regions with increasing propofol dosage. This may reflect the nonuniform effects of anesthesia on brain topologic organization.[65,70–72]

Further analysis demonstrated that metabolic connectivity strength was closely related to standardized uptake value ratio during mild sedation, indicating tight coupling between functional connectivity and energy consumption.[19,73] However, this tight relationship was gradually weakened during deep sedation and anesthesia, implying a dosage-dependent effect on the relationship between metabolic connectivity strength and metabolism. Because the brain must receive an adequate energy supply to maintain normal functions such as synaptic transmission and communication,[74] the propofol-induced decreased cerebral metabolism may be insufficient to support functional connectivity between distinct regions. Furthermore, the reduced correlation between metabolic connectivity strength and standardized uptake value ratio during deep anesthesia was accompanied by decreases in energy efficiency, indicating that the rat brain uses energy for functional communication less efficiently during propofol-induced loss of consciousness. The principle of energy efficiency has been used to study the energy cost of functional connectivity, based on the ratio between the metabolic connectivity of brain regions and energy consumption. In fact, 85% of total brain energy consumption in the awake state is devoted to neuronal communication,[75] whereas the remaining 15% is reserved for cellular homeostasis.[76] This led us to hypothesize that the brain tends to preserve its energy budget for basic cellular functions rather than for functional connectivity when cerebral metabolism is depressed by propofol, leading to a decrease in energy efficiency. It follows that the reduction in energy efficiency was not likely a reflection of mathematical fact but rather of the underlying efficient use of glucose for functional connectivity.

Analyses into the small-world topology of the metabolic brain network have shown additional insights into network dysregulation during anesthesia.[77–80] Although the brain networks retained their small-world topology during deep anesthesia, both the global and local efficiency of the metabolic brain network deteriorated with deepening anesthesia levels. Global efficiency reflects effective information transformation across remote cortical regions, which is believed

to form the basis of many cognitive processes. Local efficiency predominantly depends on connections between neighboring regions that mediate the modularized information processing and fault tolerance of a network.[43] Thus, one could speculate that increased propofol dosages cause widespread loss of functional interactions between spatially remote brain regions, giving rise to decreased global and local efficiency, which is probably responsible for the disruptions in information processing and cognitive ability during anesthesia.[16,81]

Limitations

There were several limitations in the present study. First, we did not measure the plasma concentration of propofol or monitor scalp electroencephalogram in all rats, so the level of consciousness in different rats may have been slightly different under the same propofol dosage. Second, the fluorodeoxyglucose positron emission tomography data were obtained under 1% isoflurane anesthesia to limit head movement, which may have influenced the metabolic signals. However, metabolic activity measured using [^{18}F]fluorodeoxyglucose positron emission tomography reflects cumulative energy consumption within the presumed steady resting state,[61] so positron emission tomography signals after 40 min of brain equilibrium are unlikely to be affected by isoflurane in this context. Third, the present study revealed the metabolic patterns of the $GABA_A$-enhancing anesthetic propofol. In contrast, ketamine, an *N*-methyl-D-aspartate–receptor antagonist, increases cerebral metabolism in most brain regions.[82,83] Future studies should examine whether the disrupted metabolic patterns observed during propofol-induced alterations of consciousness are drug-dependent or state-dependent.

Based on our results, we concluded that anesthetic-induced unconsciousness is correlated with disruptions to the metabolic network, although the causal direction remains unclear. Further research is needed to elucidate whether this state-related change in the metabolic network reverses after recovery from anesthesia. Such research would validate and extend the conclusions of the present study.

Finally, unlike functional magnetic resonance imaging, which is collected in the order of seconds, stationary positron emission tomography measurement of brain metabolism activity is restricted because it has poor temporal resolution—over minutes to hours. As such, we carried out correlational analyses between different brain regions across rats at the group level. This is a well accepted method to analyze anatomical connectivity networks[84,85] and metabolic networks.[38,86] However, the across-rat analysis and nonparametric permutation test between groups may limit further analysis and affect confidence in related results. Further studies should investigate the brain metabolism network during anesthesia using within-subject metabolic connectivity analysis with dynamic positron emission tomography acquisition.[87,88] Because electroencephalogram is a more direct tool to measure neuronal activity, it is important that researchers directly evaluate the relationship between electroencephalogram-derived and metabolism-derived networks in future studies by simultaneously acquiring electroencephalogram data and metabolism signals.

Conclusions

In summary, we found state-related alterations in the spatial and topologic organization of metabolic brain systems induced by increasing dosages of propofol. We also revealed a close relationship between metabolic connectivity and cerebral metabolism and that this relationship is modulated by changes in anesthesia level. These findings may provide novel insights into the metabolic mechanisms of anesthetic-induced loss of consciousness.

Acknowledgments

The authors thank Liqin Yang, Ph.D., Department of Radiology, Huashan Hospital, Fudan University, China, and Jianfeng Zhang, Ph.D., College of Biomedical Engineering and Instrument Sciences, Zhejiang University, China, for their important suggestions on data analysis.

Research Support

Supported by the Medical Guidance Supporting Project under grant No. 17411961400 (to Dr. Zhang) from the Municipal Science and Technology Committee, Shanghai, China, by the Fundamental Research Funds for the Central Universities of China (Beijing, China; to Dr. Liang), and by Natural Science Foundation of China grant No. 81671769 (Beijing, China; to Dr. Liang).

Competing Interests

The authors declare no competing interests.

Correspondence

Address correspondence to Dr. Zhang: Huashan Hospital, Fudan University, No. 12 Wulumuqi Middle Road, Jin'an District, Shanghai, China 200040. snapzhang@aliyun.com.

References

1. Maekawa T, Tommasino C, Shapiro HM, Keifer-Goodman J, Kohlenberger RW: Local cerebral blood flow and glucose utilization during isoflurane anesthesia in the rat. ANESTHESIOLOGY 1986; 65:144–51
2. Shimoji K, Ravasi L, Schmidt K, Soto-Montenegro ML, Esaki T, Seidel J, Jagoda E, Sokoloff L, Green MV, Eckelman WC: Measurement of cerebral glucose

metabolic rates in the anesthetized rat by dynamic scanning with ^{18}F-FDG, the ATLAS small animal PET scanner, and arterial blood sampling. J Nucl Med 2004; 45:665–72
3. Hudetz AG: General anesthesia and human brain connectivity. Brain Connect 2012; 2:291–302
4. Shulman RG, Hyder F, Rothman DL: Baseline brain energy supports the state of consciousness. Proc Natl Acad Sci U S A 2009; 106:11096–101
5. Fiset P, Paus T, Daloze T, Plourde G, Meuret P, Bonhomme V, Hajj-Ali N, Backman SB, Evans AC: Brain mechanisms of propofol-induced loss of consciousness in humans: A positron emission tomographic study. J Neurosci 1999; 19:5506–13
6. Alkire MT, Miller J: General anesthesia and the neural correlates of consciousness. Prog Brain Res 2005; 150:229–44
7. Alkire MT, Hudetz AG, Tononi G: Consciousness and anesthesia. Science 2008; 322:876–80
8. Tononi G, Koch C: The neural correlates of consciousness: An update. Ann NY Acad Sci 2008; 1124:239–61
9. Boveroux P, Vanhaudenhuyse A, Bruno MA, Noirhomme Q, Lauwick S, Luxen A, Degueldre C, Plenevaux A, Schnakers C, Phillips C, Brichant JF, Bonhomme V, Maquet P, Greicius MD, Laureys S, Boly M: Breakdown of within- and between-network resting state functional magnetic resonance imaging connectivity during propofol-induced loss of consciousness. Anesthesiology 2010; 113:1038–53
10. Lewis LD, Weiner VS, Mukamel EA, Donoghue JA, Eskandar EN, Madsen JR, Anderson WS, Hochberg LR, Cash SS, Brown EN, Purdon PL: Rapid fragmentation of neuronal networks at the onset of propofol-induced unconsciousness. Proc Natl Acad Sci U S A 2012; 109:E3377–86
11. Tononi G: Integrated information theory of consciousness: An updated account. Arch Ital Biol 2012; 150:56–90
12. Oizumi M, Albantakis L, Tononi G: From the phenomenology to the mechanisms of consciousness: Integrated Information Theory 3.0. PLoS Comput Biol 2014; 10:e1003588
13. Tononi G, Boly M, Massimini M, Koch C: Integrated information theory: From consciousness to its physical substrate. Nat Rev Neurosci 2016; 17:450–61
14. Lee U, Kim S, Noh GJ, Choi BM, Hwang E, Mashour GA: The directionality and functional organization of frontoparietal connectivity during consciousness and anesthesia in humans. Conscious Cogn 2009; 18:1069–78
15. Ferrarelli F, Massimini M, Sarasso S, Casali A, Riedner BA, Angelini G, Tononi G, Pearce RA: Breakdown in cortical effective connectivity during midazolam-induced loss of consciousness. Proc Natl Acad Sci U S A 2010; 107:2681–6
16. Liu X, Lauer KK, Ward BD, Rao SM, Li SJ, Hudetz AG: Propofol disrupts functional interactions between sensory and high-order processing of auditory verbal memory. Hum Brain Mapp 2012; 33:2487–98
17. Lee U, Ku S, Noh G, Baek S, Choi B, Mashour GA: Disruption of frontal-parietal communication by ketamine, propofol, and sevoflurane. Anesthesiology 2013; 118:1264–75
18. Liu X, Pillay S, Li R, Vizuete JA, Pechman KR, Schmainda KM, Hudetz AG: Multiphasic modification of intrinsic functional connectivity of the rat brain during increasing levels of propofol. Neuroimage 2013; 83:581–92
19. Liang X, Zou Q, He Y, Yang Y: Coupling of functional connectivity and regional cerebral blood flow reveals a physiological basis for network hubs of the human brain. Proc Natl Acad Sci U S A 2013; 110:1929–34
20. Tomasi D, Wang GJ, Volkow ND: Energetic cost of brain functional connectivity. Proc Natl Acad Sci U S A 2013; 110:13642–7
21. Horwitz B, Duara R, Rapoport SI: Intercorrelations of glucose metabolic rates between brain regions: Application to healthy males in a state of reduced sensory input. J Cereb Blood Flow Metab 1984; 4:484–99
22. Lee DS, Kang H, Kim H, Park H, Oh JS, Lee JS, Lee MC: Metabolic connectivity by interregional correlation analysis using statistical parametric mapping (SPM) and FDG brain PET; methodological development and patterns of metabolic connectivity in adults. Eur J Nucl Med Mol Imaging 2008; 35:1681–91
23. Di X, Biswal BB; Alzheimer's Disease Neuroimaging Initiative: Metabolic brain covariant networks as revealed by FDG-PET with reference to resting-state fMRI networks. Brain Connect 2012; 2:275–83
24. Lee H, Kang H, Chung MK, Kim BN, Lee DS: Persistent brain network homology from the perspective of dendrogram. IEEE Trans Med Imaging 2012; 31:2267–77
25. Fridman EA, Beattie BJ, Broft A, Laureys S, Schiff ND: Regional cerebral metabolic patterns demonstrate the role of anterior forebrain mesocircuit dysfunction in the severely injured brain. Proc Natl Acad Sci U S A 2014; 111:6473–8
26. Villien M, Wey HY, Mandeville JB, Catana C, Polimeni JR, Sander CY, Zürcher NR, Chonde DB, Fowler JS, Rosen BR, Hooker JM: Dynamic functional imaging of brain glucose utilization using fPET-FDG. Neuroimage 2014; 100:192–9
27. Chung J, Yoo K, Kim E, Na DL, Jeong Y: Glucose metabolic brain networks in early-onset *vs.* late-onset Alzheimer's disease. Front Aging Neurosci 2016; 8:159
28. Rosazza C, Andronache A, Sattin D, Bruzzone MG, Marotta G, Nigri A, Ferraro S, Rossi Sebastiano D, Porcu L, Bersano A, Benti R, Leonardi M, D'Incerti

L, Minati L; Coma Research Center, Besta Institute: Multimodal study of default-mode network integrity in disorders of consciousness. Ann Neurol 2016; 79:841–53
29. Matsumura A, Mizokawa S, Tanaka M, Wada Y, Nozaki S, Nakamura F, Shiomi S, Ochi H, Watanabe Y: Assessment of microPET performance in analyzing the rat brain under different types of anesthesia: Comparison between quantitative data obtained with microPET and *ex vivo* autoradiography. Neuroimage 2003; 20:2040–50
30. Tung A, Szafran MJ, Bluhm B, Mendelson WB: Sleep deprivation potentiates the onset and duration of loss of righting reflex induced by propofol and isoflurane. Anesthesiology 2002; 97:906–11
31. Kushikata T, Yoshida H, Kudo M, Salvadori S, Calo G, Hirota K: The effects of neuropeptide S on general anesthesia in rats. Anesth Analg 2011; 112:845–9
32. Reed SJ, Plourde G: Attenuation of high-frequency (50–200 Hz) thalamocortical EEG rhythms by propofol in rats is more pronounced for the thalamus than for the cortex. PLoS One 2015; 10:e0123287
33. Valdés-Hernández PA, Sumiyoshi A, Nonaka H, Haga R, Aubert-Vásquez E, Ogawa T, Iturria-Medina Y, Riera JJ, Kawashima R: An *in vivo* MRI template set for morphometry, tissue segmentation, and fMRI localization in rats. Front Neuroinform 2011; 5:26
34. Garrett DD, Kovacevic N, McIntosh AR, Grady CL: Blood oxygen level-dependent signal variability is more than just noise. J Neurosci 2010; 30:4914–21
35. Garrett DD, Kovacevic N, McIntosh AR, Grady CL: The importance of being variable. J Neurosci 2011; 31:4496–503
36. Dai Z, Yan C, Li K, Wang Z, Wang J, Cao M, Lin Q, Shu N, Xia M, Bi Y, He Y: Identifying and mapping connectivity patterns of brain network hubs in Alzheimer's disease. Cereb Cortex 2015; 25:3723–42
37. Zhang J, Huang Z, Chen Y, Zhang J, Ghinda D, Nikolova Y, Wu J, Xu J, Bai W, Mao Y, Yang Z, Duncan N, Qin P, Wang H, Chen B, Weng X, Northoff G: Breakdown in the temporal and spatial organization of spontaneous brain activity during general anesthesia. Hum Brain Mapp 2018; 39:2035–46
38. Choi H, Choi Y, Kim KW, Kang H, Hwang DW, Kim EE, Chung JK, Lee DS: Maturation of metabolic connectivity of the adolescent rat brain. Elife 2015; 4:e11571
39. Schwarz AJ, Danckaert A, Reese T, Gozzi A, Paxinos G, Watson C, Merlo-Pich EV, Bifone A: A stereotaxic MRI template set for the rat brain with tissue class distribution maps and co-registered anatomical atlas: Application to pharmacological MRI. Neuroimage 2006; 32:538–50
40. Calabrese E, Johnson GA, Watson C: An ontology-based segmentation scheme for tracking postnatal changes in the developing rodent brain with MRI. Neuroimage 2013; 67:375–84
41. Newman ME: Analysis of weighted networks. Phys Rev E Stat Nonlin Soft Matter Phys 2004; 70:056131
42. Wang J, Wang X, Xia M, Liao X, Evans A, He Y: GRETNA: A graph theoretical network analysis toolbox for imaging connectomics. Front Hum Neurosci 2015; 9:386
43. Latora V, Marchiori M: Efficient behavior of small-world networks. Phys Rev Lett 2001; 87:198701
44. Watts DJ, Strogatz SH: Collective dynamics of "small-world" networks. Nature 1998; 393:440–2
45. Maslov S, Sneppen K: Specificity and stability in topology of protein networks. Science 2002; 296:910–3
46. Sporns O, Zwi JD: The small world of the cerebral cortex. Neuroinformatics 2004; 2:145–62
47. Sperry MM, Kartha S, Granquist EJ, Winkelstein BA: Inter-subject FDG PET brain networks exhibit multiscale community structure with different normalization techniques. Ann Biomed Eng 2018; 46:1001–12
48. Olejnik S, Algina J: Generalized eta and omega squared statistics: Measures of effect size for some common research designs. Psychol Methods 2003; 8:434–47
49. Di Perri C, Bahri MA, Amico E, Thibaut A, Heine L, Antonopoulos G, Charland-Verville V, Wannez S, Gomez F, Hustinx R, Tshibanda L, Demertzi A, Soddu A, Laureys S: Neural correlates of consciousness in patients who have emerged from a minimally conscious state: A cross-sectional multimodal imaging study. Lancet Neurol 2016; 15:830–42
50. Bodart O, Gosseries O, Wannez S, Thibaut A, Annen J, Boly M, Rosanova M, Casali AG, Casarotto S, Tononi G, Massimini M, Laureys S: Measures of metabolism and complexity in the brain of patients with disorders of consciousness. Neuroimage Clin 2017; 14:354–62
51. Rex S, Schaefer W, Meyer PH, Rossaint R, Boy C, Setani K, Büll U, Baumert JH: Positron emission tomography study of regional cerebral metabolism during general anesthesia with xenon in humans. Anesthesiology 2006; 105:936–43
52. Schlünzen L, Juul N, Hansen KV, Cold GE: Regional cerebral blood flow and glucose metabolism during propofol anaesthesia in healthy subjects studied with positron emission tomography. Acta Anaesthesiol Scand 2012; 56:248–55
53. Schlünzen L, Juul N, Hansen KV, Gjedde A, Cold GE: Regional cerebral glucose metabolism during sevoflurane anaesthesia in healthy subjects studied with positron emission tomography. Acta Anaesthesiol Scand 2010; 54:603–9
54. Alkire MT, Haier RJ, Barker SJ, Shah NK, Wu JC, Kao YJ: Cerebral metabolism during propofol anesthesia in humans studied with positron emission

tomography. Anesthesiology 1995; 82:393–403; discussion 27A
55. Toyama H, Ichise M, Liow JS, Modell KJ, Vines DC, Esaki T, Cook M, Seidel J, Sokoloff L, Green MV, Innis RB: Absolute quantification of regional cerebral glucose utilization in mice by ^{18}F-FDG small animal PET scanning and 2-^{14}C-DG autoradiography. J Nucl Med 2004; 45:1398–405
56. Alf MF, Duarte JM, Lei H, Krämer SD, Mlynarik V, Schibli R, Gruetter R: MRS glucose mapping and PET joining forces: Re-evaluation of the lumped constant in the rat brain under isoflurane anaesthesia. J Neurochem 2014; 129:672–82
57. Franks NP: General anaesthesia: From molecular targets to neuronal pathways of sleep and arousal. Nat Rev Neurosci 2008; 9:370–86
58. Brown EN, Purdon PL, Van Dort CJ: General anesthesia and altered states of arousal: A systems neuroscience analysis. Annu Rev Neurosci 2011; 34:601–28
59. Braestrup C, Albrechtsen R, Squires RF: High densities of benzodiazepine receptors in human cortical areas. Nature 1977; 269:702–4
60. Zou N, Chetelat G, Baydogan MG, Li J, Fischer FU, Titov D, Dukart J, Fellgiebel A, Schreckenberger M, Yakushev I: Metabolic connectivity as index of verbal working memory. J Cereb Blood Flow Metab 2015; 35:1122–6
61. Yakushev I, Drzezga A, Habeck C: Metabolic connectivity: Methods and applications. Curr Opin Neurol 2017; 30:677–85
62. Eckert T, Tang C, Eidelberg D: Assessment of the progression of Parkinson's disease: A metabolic network approach. Lancet Neurol 2007; 6:926–32
63. Yakushev I, Chételat G, Fischer FU, Landeau B, Bastin C, Scheurich A, Perrotin A, Bahri MA, Drzezga A, Eustache F, Schreckenberger M, Fellgiebel A, Salmon E: Metabolic and structural connectivity within the default mode network relates to working memory performance in young healthy adults. Neuroimage 2013; 79:184–90
64. Sala A, Caminiti SP, Presotto L, Premi E, Pilotto A, Turrone R, Cosseddu M, Alberici A, Paghera B, Borroni B, Padovani A, Perani D: Altered brain metabolic connectivity at multiscale level in early Parkinson's disease. Sci Rep 2017; 7:4256
65. Schröter MS, Spoormaker VI, Schorer A, Wohlschläger A, Czisch M, Kochs EF, Zimmer C, Hemmer B, Schneider G, Jordan D, Ilg R: Spatiotemporal reconfiguration of large-scale brain functional networks during propofol-induced loss of consciousness. J Neurosci 2012; 32:12832–40
66. Huang Z, Wang Z, Zhang J, Dai R, Wu J, Li Y, Liang W, Mao Y, Yang Z, Holland G, Zhang J, Northoff G: Altered temporal variance and neural synchronization of spontaneous brain activity in anesthesia. Hum Brain Mapp 2014; 35:5368–78
67. Huang Z, Zhang J, Wu J, Qin P, Wu X, Wang Z, Dai R, Li Y, Liang W, Mao Y, Yang Z, Zhang J, Wolff A, Northoff G: Decoupled temporal variability and signal synchronization of spontaneous brain activity in loss of consciousness: An fMRI study in anesthesia. Neuroimage 2016; 124:693–703
68. Stamatakis EA, Adapa RM, Absalom AR, Menon DK: Changes in resting neural connectivity during propofol sedation. PLoS One 2010; 5:e14224
69. Lee U, Mashour GA: Role of network science in the study of anesthetic state transitions. Anesthesiology 2018; 129:1029–44
70. Ku SW, Lee U, Noh GJ, Jun IG, Mashour GA: Preferential inhibition of frontal-to-parietal feedback connectivity is a neurophysiologic correlate of general anesthesia in surgical patients. PLoS One 2011; 6:e25155
71. Blain-Moraes S, Lee U, Ku S, Noh G, Mashour GA: Electroencephalographic effects of ketamine on power, cross-frequency coupling, and connectivity in the alpha bandwidth. Front Syst Neurosci 2014; 8:114
72. Bonhomme V, Vanhaudenhuyse A, Demertzi A, Bruno MA, Jaquet O, Bahri MA, Plenevaux A, Boly M, Boveroux P, Soddu A, Brichant JF, Maquet P, Laureys S: Resting-state network-specific breakdown of functional connectivity during ketamine alteration of consciousness in volunteers. Anesthesiology 2016; 125:873–88
73. Fukunaga M, Horovitz SG, de Zwart JA, van Gelderen P, Balkin TJ, Braun AR, Duyn JH: Metabolic origin of BOLD signal fluctuations in the absence of stimuli. J Cereb Blood Flow Metab 2008; 28:1377–87
74. Hyder F, Sanganahalli BG, Herman P, Coman D, Maandag NJ, Behar KL, Blumenfeld H, Rothman DL: Neurovascular and neurometabolic couplings in dynamic calibrated fMRI: Transient oxidative neuroenergetics for block-design and event-related paradigms. Front Neuroenergetics 2010; 2:18
75. Shulman RG, Hyder F, Rothman DL: Insights from neuroenergetics into the interpretation of functional neuroimaging: An alternative empirical model for studying the brain's support of behavior. J Cereb Blood Flow Metab 2014; 34:1721–35
76. Hyder F, Fulbright RK, Shulman RG, Rothman DL: Glutamatergic function in the resting awake human brain is supported by uniformly high oxidative energy. J Cereb Blood Flow Metab 2013; 33:339–47
77. Lee U, Müller M, Noh GJ, Choi B, Mashour GA: Dissociable network properties of anesthetic state transitions. Anesthesiology 2011; 114:872–81
78. Kuhlmann L, Foster BL, Liley DT: Modulation of functional EEG networks by the NMDA antagonist nitrous oxide. PLoS One 2013; 8:e56434
79. Kim M, Mashour GA, Moraes SB, Vanini G, Tarnal V, Janke E, Hudetz AG, Lee U: Functional and topological

conditions for explosive synchronization develop in human brain networks with the onset of anesthetic-induced unconsciousness. Front Comput Neurosci 2016; 10:1

80. Hashmi JA, Loggia ML, Khan S, Gao L, Kim J, Napadow V, Brown EN, Akeju O: Dexmedetomidine disrupts the local and global efficiencies of large-scale brain networks. Anesthesiology 2017; 126:419–30
81. Monti MM, Lutkenhoff ES, Rubinov M, Boveroux P, Vanhaudenhuyse A, Gosseries O, Bruno MA, Noirhomme Q, Boly M, Laureys S: Dynamic change of global and local information processing in propofol-induced loss and recovery of consciousness. PLoS Comput Biol 2013; 9:e1003271
82. Långsjö JW, Maksimow A, Salmi E, Kaisti K, Aalto S, Oikonen V, Hinkka S, Aantaa R, Sipilä H, Viljanen T, Parkkola R, Scheinin H: *S*-Ketamine anesthesia increases cerebral blood flow in excess of the metabolic needs in humans. Anesthesiology 2005; 103:258–68
83. Långsjö JW, Salmi E, Kaisti KK, Aalto S, Hinkka S, Aantaa R, Oikonen V, Viljanen T, Kurki T, Silvanto M, Scheinin H: Effects of subanesthetic ketamine on regional cerebral glucose metabolism in humans. Anesthesiology 2004; 100:1065–71
84. Lerch JP, Worsley K, Shaw WP, Greenstein DK, Lenroot RK, Giedd J, Evans AC: Mapping anatomical correlations across cerebral cortex (MACACC) using cortical thickness from MRI. Neuroimage 2006; 31:993–1003
85. He Y, Chen ZJ, Evans AC: Small-world anatomical networks in the human brain revealed by cortical thickness from MRI. Cereb Cortex 2007; 17:2407–19
86. Choi H, Kim YK, Kang H, Lee H, Im HJ, Hwang DW, Kim EE, Chung JK, Lee DS: Abnormal metabolic connectivity in the pilocarpine-induced epilepsy rat model: A multiscale network analysis based on persistent homology. Neuroimage 2014; 99:226–36
87. Passow S, Specht K, Adamsen TC, Biermann M, Brekke N, Craven AR, Ersland L, Grüner R, Kleven-Madsen N, Kvernenes OH, Schwarzlmüller T, Olesen RA, Hugdahl K: Default-mode network functional connectivity is closely related to metabolic activity. Hum Brain Mapp 2015; 36:2027–38
88. Tomasi DG, Shokri-Kojori E, Wiers CE, Kim SW, Demiral ŞB, Cabrera EA, Lindgren E, Miller G, Wang GJ, Volkow ND: Dynamic brain glucose metabolism identifies anti-correlated cortical-cerebellar networks at rest. J Cereb Blood Flow Metab 2017; 37:3659–70